SUPPORTING INFORMATION

Robust Route to Photocatalytic Nitrogen Fixation Mediated by Capitalizing on Defect-Tailoring $InVO_4$ Nanosheets

*Shan Yao [a], Jiawen Liu [a], Fangyan Liu [a], Biao Wang [a], Ying Ding [a], Li Li[*e], Chuan Liu [c], Feng Huang [a], Jingyun Fang [d], Zhang Lin [b] and Mengye Wang [*a]*

[a] *School of Materials, Sun Yat-Sen University, Shenzhen 518107, State Key Laboratory of Optoelectronic Materials and Technologies, Sun Yat-Sen University, Guangzhou 510275, China.*

[b] *School of Metallurgy and Environment, Central South University, Changsha, Hunan, 410083. School of Environment and Energy, Guangdong Provincial Key Laboratory of Solid Wastes Pollution Control and Recycling, South China University of Technology, Guangzhou 510006, China.*

[c] *The Guangdong Province Key Laboratory of Display Material and Technology, School of Electronics and Information Technology, Sun Yat-Sen University, Guangzhou 510275, China.*

[d] *Guangdong Provincial Key Laboratory of Environmental Pollution Control and Remediation Technology, School of Environmental Science and Engineering, Sun Yat-Sen University, Guangzhou 510275, China.*

[e] *School of Environment and Energy, Guangdong Provincial Key Laboratory of Solid Wastes Pollution Control and Recycling, South China University of Technology, Guangzhou 510006, China.*

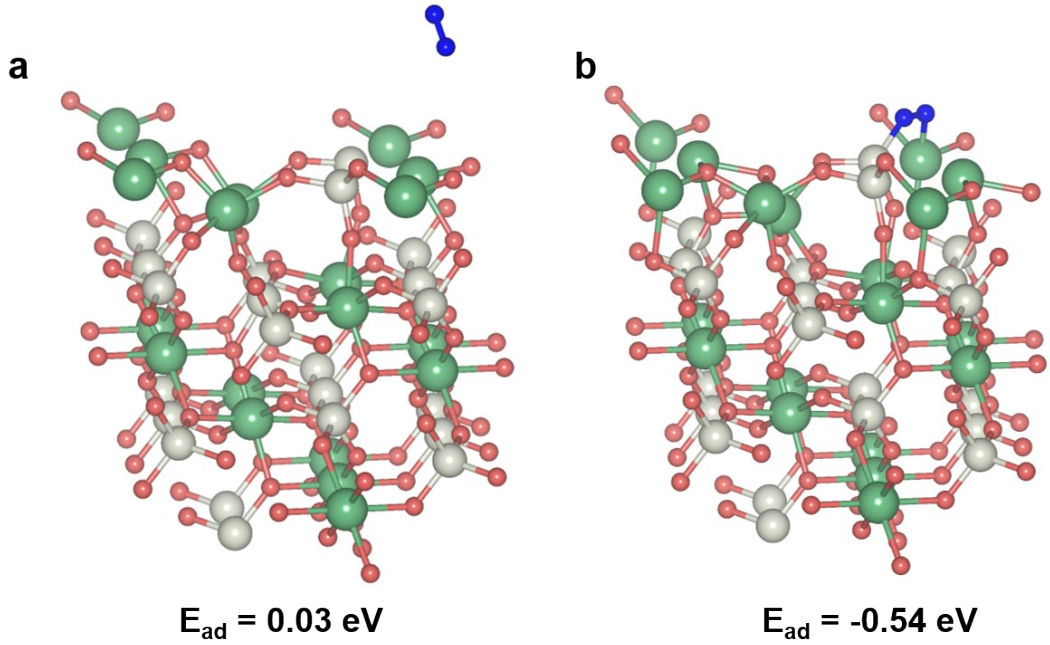

Figure S1. Calculated model and corresponding energy of a N_2 molecule adsorbed on (a) the top site of In atom and (b) the bridge site between In and V atom.

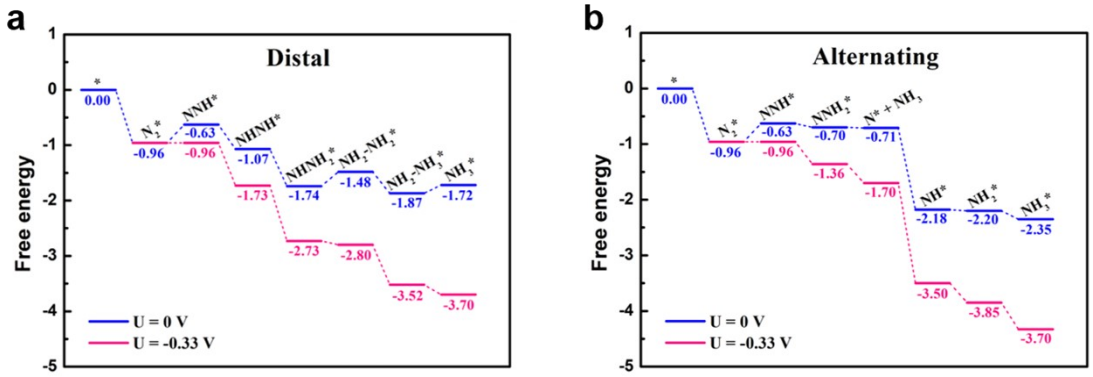

Figure S2. Free energy diagrams for N_2 reduction through (a) distal, (b) alternating mechanisms at U= 0 V and -0.33 V, respectively.

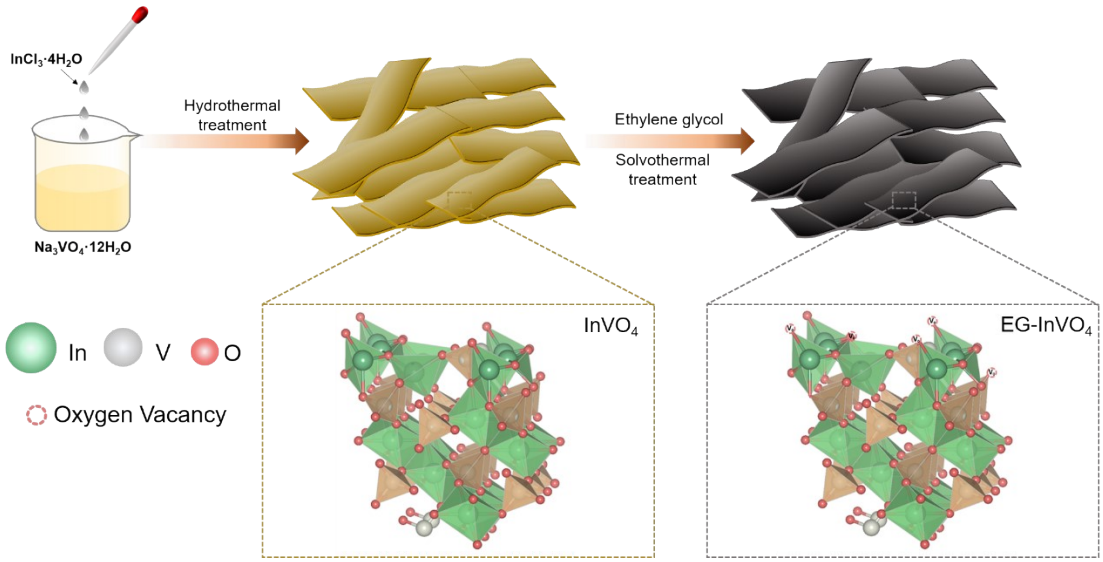

Figure S3. Schematic synthetic route of $InVO_4$ and EG-$InVO_4$ nanosheets. $InVO_4$ nanosheets were synthesized via a mild hydrothermal method. Then the obtained samples were dispersed in the reducing agent (i.e., ethylene glycol). At last, the $InVO_4$ photocatalysts rich in oxygen vacancies could be obtained after a solvothermal treatment.

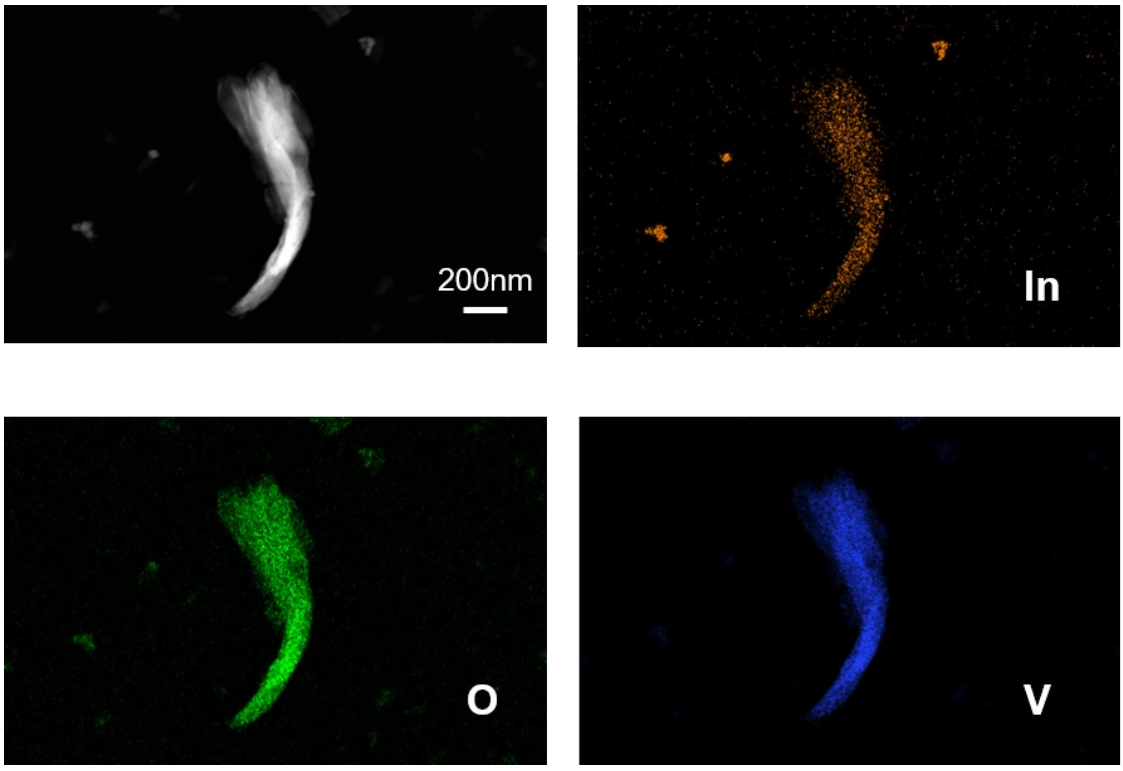

Figure S4. STEM image and EDS element mapping profiles of $InVO_4$ with In, O, and V distribution.

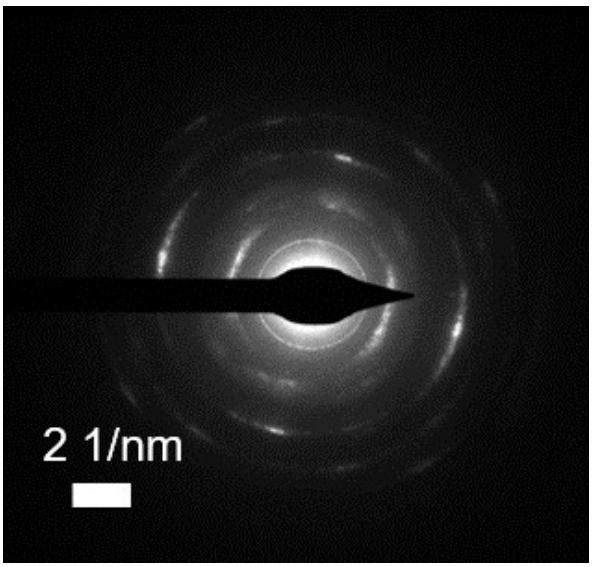

Figure S5. SAED patterns of EG10h-$InVO_4$

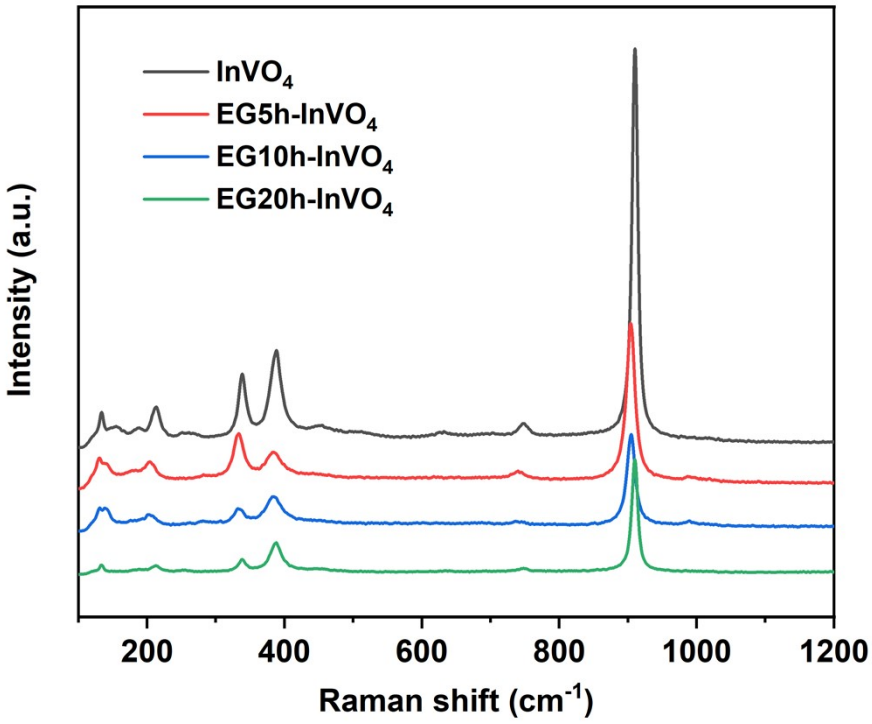

Figure S6. Raman patterns of $InVO_4$ with different solvothermal treatment times. The Raman peaks for all the samples can be well indexed to the $InVO_4$, indicating that the introduction of oxygen vacancies does not alter the crystal phase.

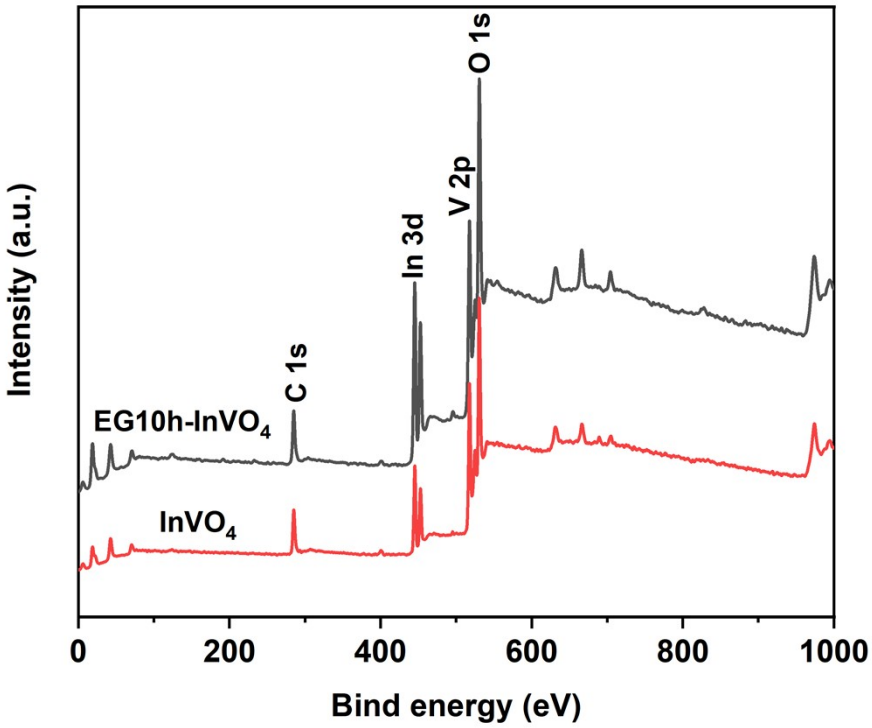

Figure S7. XPS survey spectra of $InVO_4$ and EG10h-$InVO_4$.

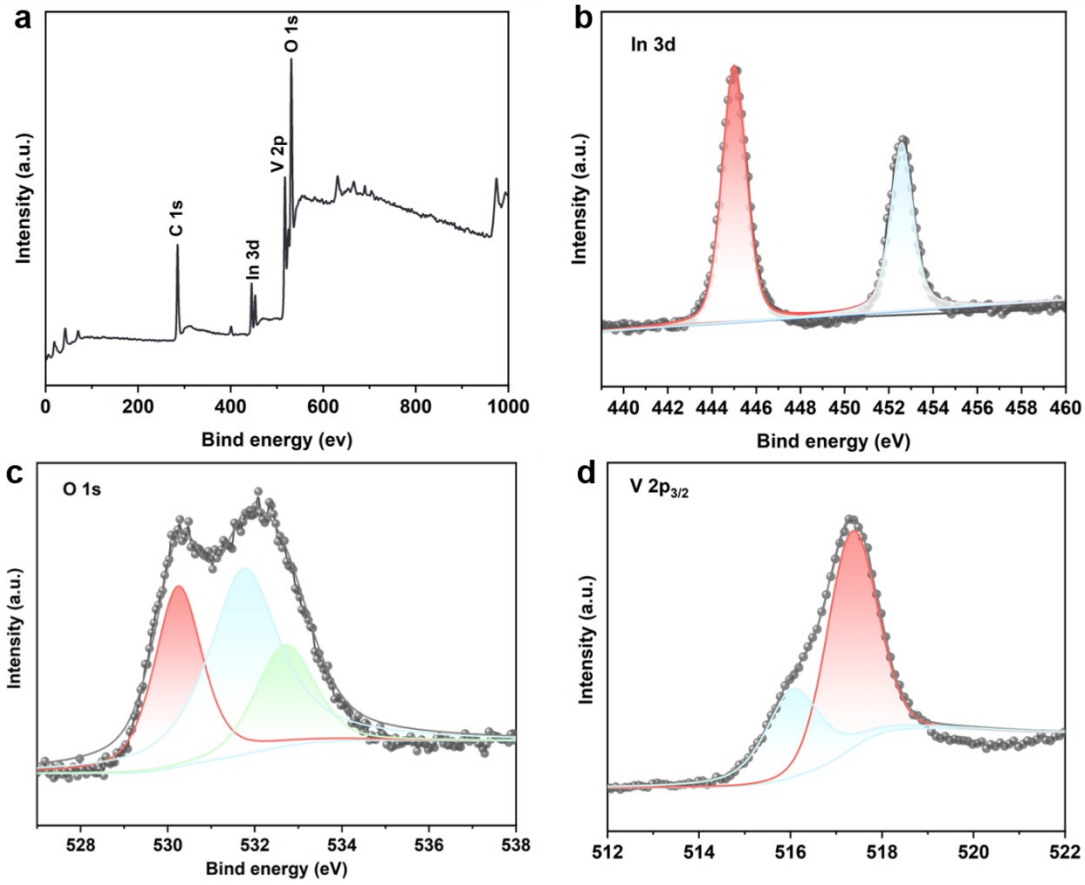

Figure S8. (a) XPS survey spectra of EG20h-$InVO_4$. High-resolution XPS spectra of (b) In 3d, (c) O 1s, and (d) V $2p_{3/2}$ of EG20h-$InVO_4$.

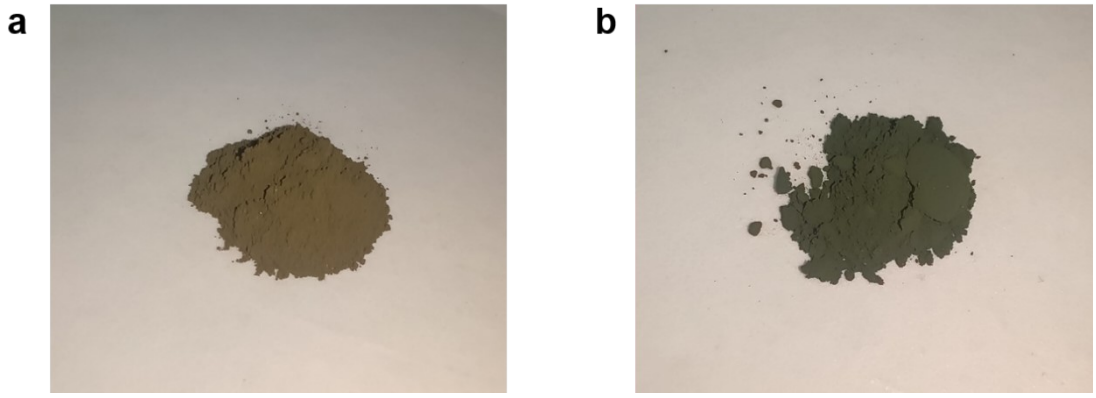

Figure S9. Digital image of (a) $InVO_4$ and (b) EG10h-$InVO_4$.

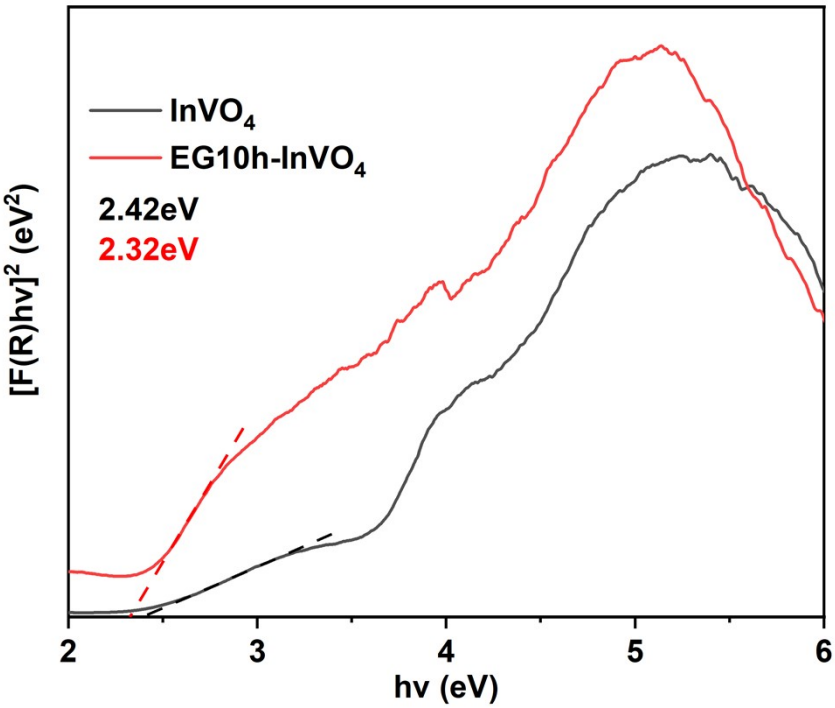

Figure S10. Tauc plots of $InVO_4$ and EG10h-$InVO_4$.

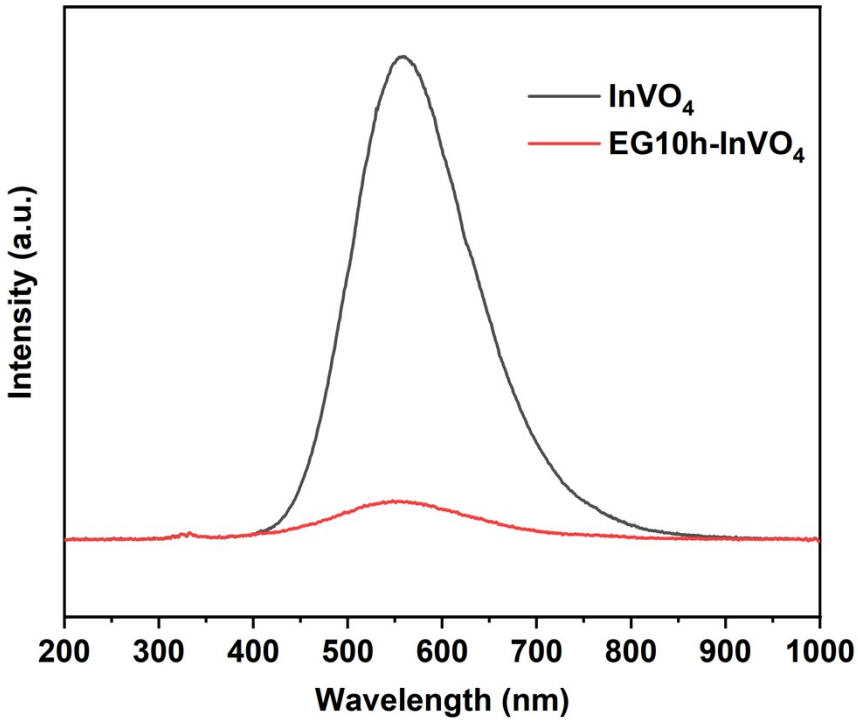

Figure S11. PL spectra of pristine $InVO_4$ and EG10h-$InVO_4$.

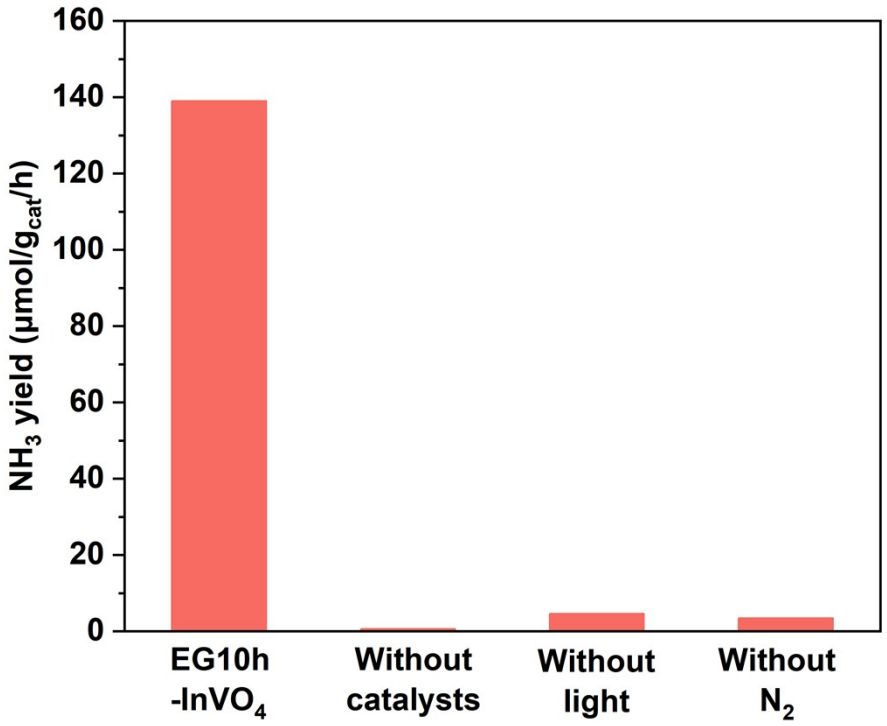

Figure S12. Control experiments under different conditions.

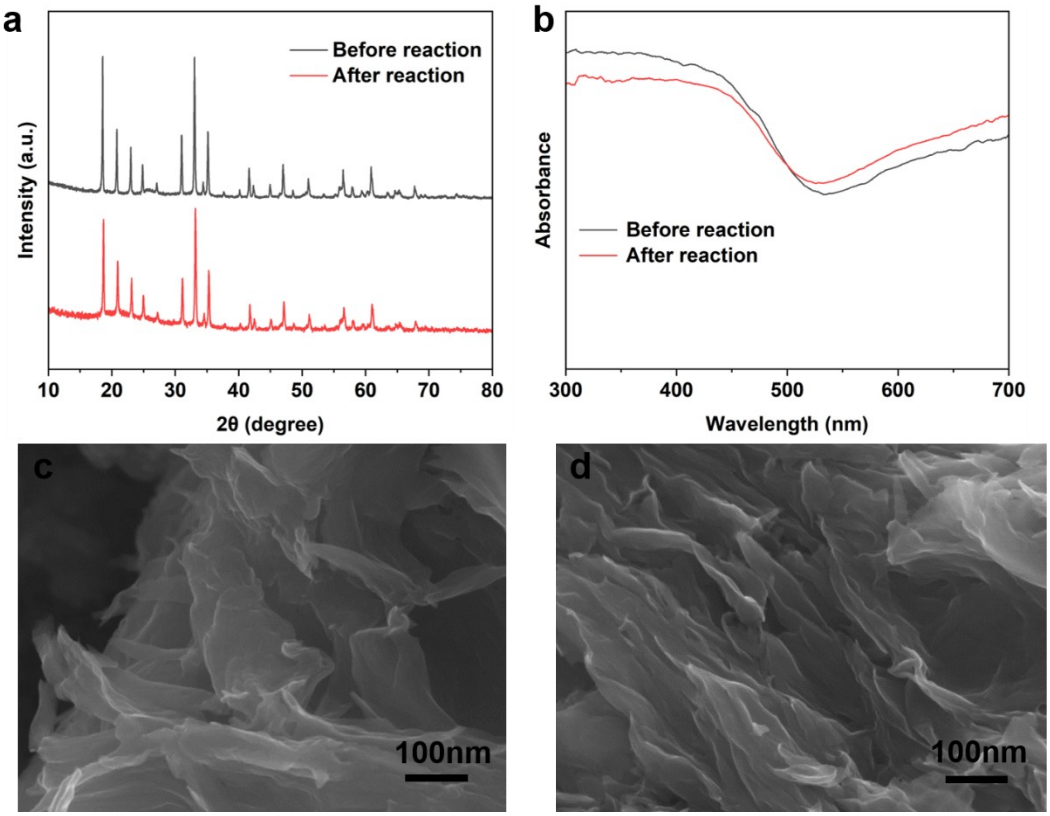

Figure S13. (a) XRD patterns, (b) UV-vis absorption spectra of EG10h-$InVO_4$ before and after the photocatalytic reaction. SEM images of the EG 10h-$InVO_4$ nanosheets (c) before and (d) after the photocatalytic reaction.

Table S1. Specific surface areas of different samples

Samples	Specific Surface Area (m^2/g)
$InVO_4$	2.3271
EG5h-$InVO_4$	3.0307
EG10h-$InVO_4$	5.2493
EG20h-$InVO_4$	2.6351

Table S2. The ratio of V^{5+}, V^{4+} and different types of oxygen in $InVO_4$, EG10h-$InVO_4$ and EG20h-$InVO_4$ reckoned by XPS.

	V^{5+}	V^{4+}	lattice oxygen	oxygen vacancy	surface oxygen
$InVO_4$	83.46%	16.54%	92.04%	4.78%	3.18%
EG10h-$InVO_4$	65.13%	34.87%	62.05%	26.41%	11.54%
EG20h-$InVO_4$	74.94%	25.06%	30.2%	50.64%	19.16%